Diffusion kinetics originating a bifurcation of the final states in the phase separation of the $Ni_3Al_{1-x}V_x$ alloy system

2005 J. Phys.: Condens. Matter 17 4911

(http://iopscience.iop.org/0953-8984/17/32/005)

INSTITUTE OF PHYSICS PUBLISHING JOURNAL OF PHYSICS: CONDENSED MATTER

J. Phys.: Condens. Matter **17** (2005) 4911–4924 doi:10.1088/0953-8984/17/32/005

Diffusion kinetics originating a bifurcation of the final states in the phase separation of the $Ni_3Al_{1-x}V_x$ alloy system

Makoto Tanimura[1,3] **and Yasumasa Koyama**[2]

[1] Research Department, NISSAN ARC, LTD, Yokosuka, Kanagawa 237-0061, Japan
[2] Kagami Memorial Laboratory for Materials Science and Technology and Department of Materials Science and Engineering, Waseda University, Shinjuku, Tokyo 169-8555, Japan

E-mail: tanimura@nissan-arc.co.jp

Received 15 April 2005, in final form 23 June 2005
Published 29 July 2005
Online at stacks.iop.org/JPhysCM/17/4911

Abstract

The evolution of states related to $D0_{22}$ precipitation in the supersaturated $L1_2$ matrix to form the $L1_2 + D0_{22}$ equilibrium state of the $Ni_3Al_{1-x}V_x$ ($0.40 \leqslant x \leqslant 0.60$) alloy system was examined by transmission electron microscopy. Our results revealed that the microstructure of the initial $L1_2$ single state varied with the change in the alloy composition and that such a variation caused a bifurcation of the final states, i.e., the $L1_2 + D0_{22}$ equilibrium state ($x = 0.40$ and $x \geqslant 0.55$) and the metastable $L1_2$ single state ($0.40 < x < 0.55$). It was also found that three types of kinetic processes originated from the variation of the initial microstructure and led to the final bifurcation. A key factor causing the difference in the kinetic processes was thought to be the sensitivity of the atomic migration paths to a decrease in the crucial vacant sites in the $L1_2$ matrix from supersaturated to equilibrium ones during the isothermal process. The final bifurcation due to such sensitivity strongly suggests that the diffusion kinetics should be treated as an 'open system' in terms of the annihilation of vacancies under the present thermodynamic conditions.

1. Introduction

Phase separation from a metastable state is a well-known phenomenon in alloys, and many studies have been carried out to date concerning the kinetics of phase separation. The basic principle of phase separation is generally understood to be a minimization of the free energy in a closed system. Thus, phase separation is an irreversible relaxation phenomenon and the final state that the system should head for is one of equilibrium under a given thermodynamic condition. As is well known, the mechanism of phase separation can be classified broadly into two categories, i.e., nucleation-growth and spinodal decompositions. Because both types of

[3] Author to whom any correspondence should be addressed.

0953-8984/05/324911+14$30.00

phase separation occur depending on the distribution of the chemical composition, the kinetics is basically controlled by the long-range atomic diffusion.

It has been widely accepted that point defects play a crucial role in the atomic diffusion in alloys. One well-known model for explaining the diffusion kinetics is the site exchange between atoms and vacancies. At the same time, another view of this model is that an atom at a site cannot jump to adjacent sites that are already occupied by other atoms. This implies that the diffusion kinetics largely depends on the local atomic environment, i.e., the configuration of atoms and vacancies. Interesting physics arises theoretically when the diffusion kinetics is strictly interpreted by a stochastic analysis based on atomistic models [1, 2]. That is, time averaging and ensemble averaging of the observable quantities such as the correlation factor in the diffusion process are not equivalent if the diffusion field exhibits a severe selectivity of atomic jump sites. An appropriate example to illustrate the constraint on diffusion is an ordered structure, where the degrees of freedom of atomic jumps are reduced due to the preferential vacant sites as well as the regular atomic arrangement. In line with this viewpoint, the diffusion kinetics in ordered structures of alloys is worthy of attention.

Very recently, we found that $D0_{22}$ (Ni_3V) precipitation in the supersaturated $L1_2$ (Ni_3Al) matrix leading to the formation of the $L1_2 + D0_{22}$ equilibrium state stagnated in the $Ni_3Al_{0.52}V_{0.48}$ alloy under a given isothermal process [3, 4]. Note that the $D0_{22}$ and $L1_2$ structures are A_3B-type ordered ones based on the fcc lattice and that the precipitation is basically controlled by the diffusion of the V atoms. A characteristic of the evolution of states during the stagnation is the transient appearance of the $D0_{22}$ regions in the $L1_2$ matrix ($L1_2$–$L1_2 + D0_{22}$–$L1_2$), accompanied by reversible-like atomic migration. This extraordinary atomic migration is attributed to diffusion blocking due to fewer vacancies on the B sites than on the A sites of the $L1_2$ ordered structure [4–8]. Deviation of the final state from the $L1_2 + D0_{22}$ equilibrium state suggests that the severe selectivity of atomic jump sites in the $L1_2$ structure influences the evolution of states of the $Ni_3Al_{0.52}V_{0.48}$ alloy. It is obvious that the peculiar evolution of states is based upon the nonequivalence between the two averaging approaches in the diffusion flow that has been pointed out theoretically.

In this study, in order to obtain a better understanding of the phase separation of the $Ni_3Al_{1-x}V_x$ alloy system, the temporal evolution of states in the phase separation of alloys with $0.40 \leqslant x \leqslant 0.60$ was examined by transmission electron microscopy. As a result, we have found that the variation in the initial microstructures of the alloys determines the respective kinetic processes in the evolution of states and that differences in the processes cause a bifurcation of the final states, i.e., the $L1_2 + D0_{22}$ equilibrium state ($x = 0.40$ and $x \geqslant 0.55$) and the metastable $L1_2$ single state ($0.40 < x < 0.55$) under the present thermodynamic treatment. The details of the experimental results and the diffusion kinetics originating this peculiar bifurcation will be given below.

2. Experimental procedure

Ingots of $Ni_3Al_{1-x}V_x$ alloys with $0.40 \leqslant x \leqslant 0.60$ were made by an Ar-arc melting technique. The chemical compositions of the ingots were confirmed by inductively coupled plasma spectroscopy. A heat-treatment process for inducing phase separation was determined in reference to the phase diagram of the alloy system [9]. It should be noted that the $Ni_3Al_{1-x}V_x$ alloy system possesses the typical eutectoid-type reaction field, where the eutectoid composition and temperature are $x = 0.80$ and 1281 K. Initially, all of the ingots were homogenized at 1623 K (fcc region) for 24 h, followed by quenching in ice water. As will be shown later, this quenching process did not suppress the fcc $\rightarrow L1_2$ ordering in the alloys with $x \leqslant 0.60$, resulting in the formation of the supersaturated $L1_2$ state as a metastable state.

It should be mentioned here that, in order to examine the evolution of states dominated by the diffusion kinetics in the $L1_2$ matrix, the effect of the grain boundaries on the diffusion process should be avoided as much as possible. To avoid such influence in this study, the samples were homogenized at 1623 K for 24 h to obtain large $L1_2$ grains with an average size of more than 100 μm.

When all of the quenched alloys were kept isothermally at a given temperature lower than the eutectoid temperature (the $L1_2 + D0_{22}$ region), it was presumed that $D0_{22}$ precipitation would take place in the $L1_2$ matrix to form the $L1_2 + D0_{22}$ equilibrium state. Concretely, the samples cut from the respective ingots were kept at 1173 K for up to 1000 h, followed by quenching in ice water again. After that, the features of the microstructures of the respective samples were examined by transmission electron microscopy.

Specimens for transmission electron microscope observation were made by mechanical-polishing and ion-thinning methods. The electron diffraction patterns and the microstructures of the alloys were observed by using an H-800 transmission electron microscope (200 keV). Energy dispersive x-ray (EDX) spectra were obtained by using an HF-2000 transmission electron microscope (200 keV) with an electron probe about 2 nm in diameter. The chemical compositions of the $L1_2$ matrix and the $D0_{22}$ precipitates that appeared in the respective samples were determined by using the Ni Kα, Al Kα and V Kα lines, and a measured value resolution of about $x = \pm 0.02$ was obtained.

3. Experimental results

3.1. Bifurcation of the final states in the $Ni_3Al_{1-x}V_x$ alloys with $0.40 \leqslant x \leqslant 0.60$

First of all, we will show a series of microstructures obtained from the quenched $Ni_3Al_{1-x}V_x$ alloys with $0.40 \leqslant x \leqslant 0.60$. Figure 1 displays the electron diffraction patterns and the dark-field images of the alloys obtained under the electron incidence parallel to the [001] direction (in this paper, for simplicity, all of the Miller indices are given in terms of the fcc notation). The existence of the diffraction spots at 100- and 110-type positions in the respective diffraction patterns is indicative of the occurrence of the $L1_2$ ordering in all of the quenched alloys. As shown in the dark-field images (all of which were taken by using 100 ordered spots), however, the microstructures of the $L1_2$ states differ depending on the variation of the V content. In the alloy with $x = 0.40$, the $L1_2$ single state forms, which contains many pairs of partial dislocations.

When the V content is increased to $x \geqslant 0.42$, square domains appear in the $L1_2$ matrix. As has been reported previously, the domains are cuboidal, and are divided by the small-angle tilt boundaries running along one of the $\langle 100 \rangle$ directions in the $L1_2$ matrix [3]. In conjunction with the formation of the domains, very weak intensities due to diffuse scattering can be detected at the $\frac{1}{2}$10-type positions. The appearance of such intensities at these positions implies that the short-range $D0_{22}$ ordering also occurs in the quenched alloys, together with the appearance of the domains. Detailed analyses reveal that segments of the small-angle tilt boundaries have the $D0_{22}$ atomic configuration (as an example, see the inset in the image of the alloy with $x = 0.60$). An important feature of these microstructures is that the average size of the domains diminishes with an increase in the V content. Concretely, the domain size of the alloys with $0.42 \leqslant x \leqslant 0.50$ is about 200 nm on a side, while that of the alloys with $x = 0.52$ and 0.55 is about 100 nm. A further increase in the V content reduces the size much more, for example, to about 30 nm on a side in the alloy with $x = 0.60$. Corresponding to this reduction, the relative intensities of the diffuse scattering increase, although the intensities are still very weak. This increase in intensity is attributed to an increase in the volume fraction of the $D0_{22}$ ordering segments, together with the increase in the V content. These experimental

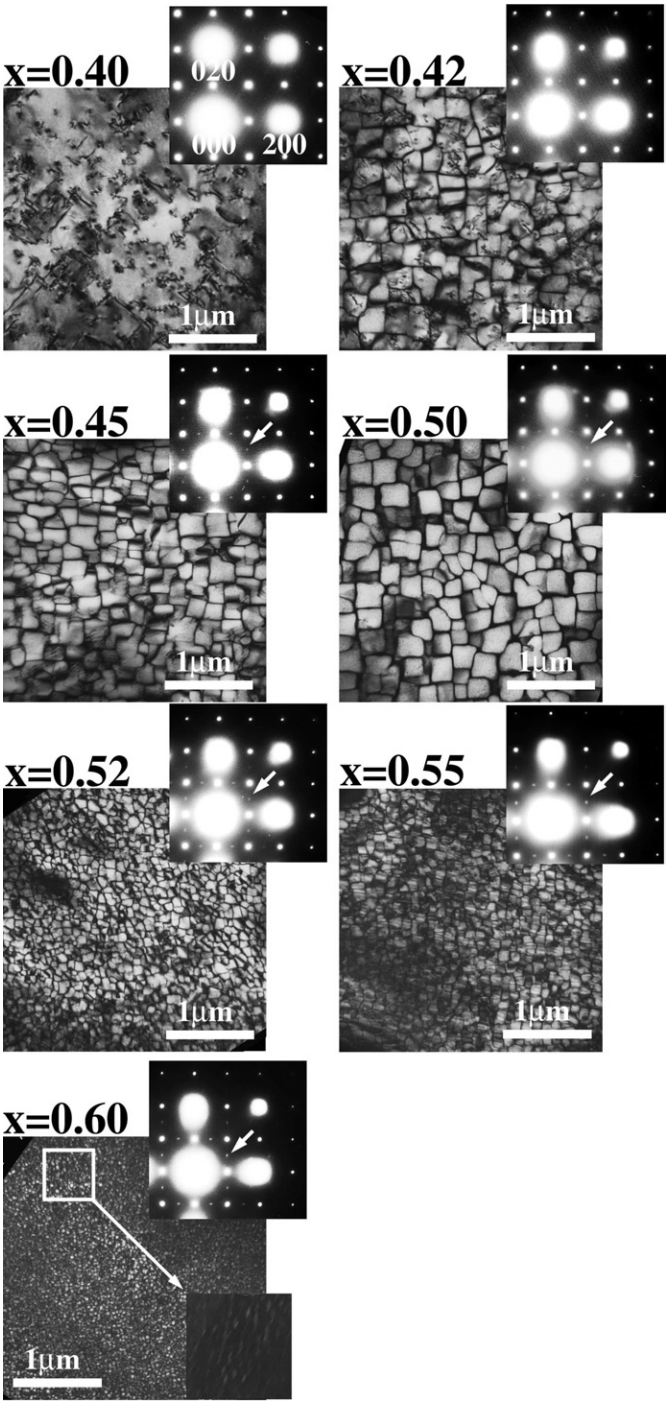

Figure 1. A series of electron diffraction patterns and dark-field images obtained from quenched $Ni_3Al_{1-x}V_x$ alloys with $0.40 \leqslant x \leqslant 0.60$. All of the images were taken by using 100 ordered spots due to the $L1_2$ structure under the electron incidence parallel to the [001] axis. In addition, a dark-field image taken by using a $\frac{1}{2}$ 10 ordered spot due to the $D0_{22}$ structure is inserted in the image obtained from the alloy with $x = 0.60$ (a magnified image of the square region).

results indicate that the microstructures of the quenched alloys continuously vary, in terms of the formation of cuboidal domains, together with the change in the V content.

We will describe here the evolution of states when all of the quenched alloys were kept at a temperature of 1173 K. Note that, according to the phase diagram, the equilibrium state of these alloys at that temperature is the $L1_2 + D0_{22}$ state. Figure 2 displays a series of images of the microstructures of the alloys kept at 1173 K for 100 h, together with the respective electron diffraction patterns.

Let us briefly examine the microstructures of the alloys with $x = 0.40$ and 0.60. The coexistence of the diffraction spots at $\frac{1}{2}10$-type positions as well as 100- and 110-type positions with strong intensities in both diffraction patterns is indicative of the formation of the $L1_2 + D0_{22}$ state. In the corresponding dark-field images taken by using $\frac{1}{2}10$ ordered spots, we can actually observe the presence of the $D0_{22}$ regions in the $L1_2$ matrix. Note that the $L1_2/D0_{22}$ habit plane is the $\{110\}$ plane. The presence of the $D0_{22}$ regions clearly implies that both alloys actually evolve to the $L1_2 + D0_{22}$ state.

The evolution of states to the equilibrium $L1_2 + D0_{22}$ state was confirmed in these two alloys, the V content of which corresponds to both ends of the composition range ($0.40 \leqslant x \leqslant 0.60$) examined in this work. Within this composition range, however, a unique evolution of states was observed. In the case of the alloys with $x = 0.42$ and 0.45, the diffraction patterns indicate that the alloys are in the $L1_2$ single state. In the corresponding dark-field images taken by using 100 ordered spots, large $L1_2$ single grains with few lattice defects are observed, while no $D0_{22}$ regions can be detected. This clearly implies that $D0_{22}$ precipitation stagnates while the alloys are kept at 1173 K, just as it does in the case of the alloy with $x = 0.48$. As for the alloy with $x = 0.50$, the diffraction pattern indicates that the alloy kept at 1173 K for 100 h is basically in the $L1_2$ single state. One important difference from the alloys with $x = 0.40$ and 0.42 is the appearance of many antiphase boundaries (APBs) in the microstructure. As has been reported previously, such APBs appear after the $D0_{22}$ regions nucleate at the small-angle tilt boundaries and are subsequently annihilated due to the change in the $L1_2/D0_{22}$ habit planes (refer to the state of the alloy with $x = 0.48$ and a 10 h hold time shown in [3]). On this basis, it is considered that the microstructure, including many APBs observed in the alloy with $x = 0.50$ and a 100 h hold time, undergoes a transition to the $L1_2$ single state. On the other hand, it is seen that the density of the APBs becomes larger in the $L1_2$ matrix as the V content of the alloy increases, as is evident in the microstructures of the alloys with $x = 0.52$ and 0.55. Additionally, the $D0_{22}$ ordered spots appear at $\frac{1}{2}10$-type positions in the diffraction patterns of both alloys, although their intensities are very weak. Actually, in the dark-field images taken by using the $\frac{1}{2}10$ spot, a very small volume fraction of the $D0_{22}$ regions can be observed in the vicinity of the APBs (as an example, see the inset in the image of the alloy with $x = 0.55$). It is thus understood that the alloys with $x = 0.52$ and 0.55 and a 100 h hold time are in the $L1_2 + D0_{22}$ state.

The final states of the alloys were confirmed by keeping them at 1173 K for up to 1000 h. Two types of final state were obtained as a result, i.e., the $L1_2 + D0_{22}$ state and the metastable $L1_2$ single state. For example, the alloys with $x = 0.42$ and 0.45 and a hold time of 100 h did not exhibit any change in their microstructures during that period. In other words, the $L1_2$ single state with few APBs can be regarded as the final state in the present isothermal process. Because the final states of the alloys with $0.50 \leqslant x \leqslant 0.55$ are still not conclusive, we will focus here on the changes in the microstructures of these alloys.

Figure 3 shows a series of electron diffraction patterns and dark-field images of the alloys with $x \geqslant 0.50$. In the alloy with $x = 0.50$, the microstructure obtained at a hold time of 500 h exhibits the $L1_2$ single state with few APBs, the same as for the 100 h hold-time alloys with $x = 0.42$ and 0.45. In the corresponding electron diffraction pattern, the $D0_{22}$ ordered spots

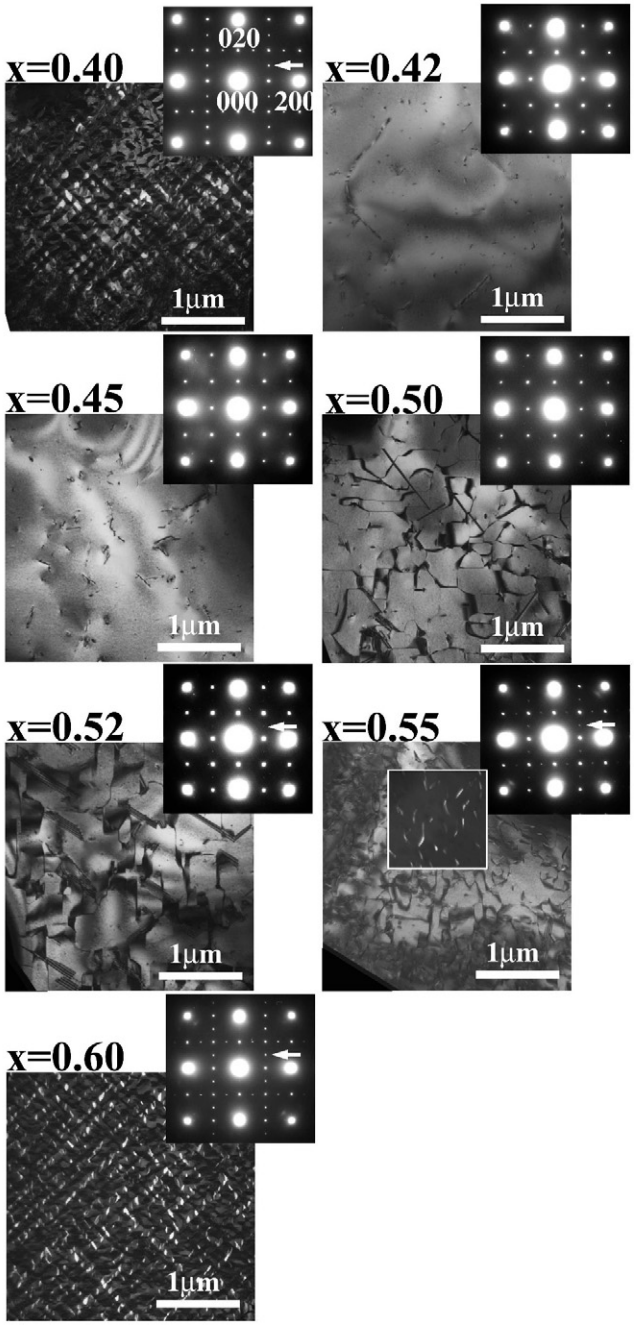

Figure 2. A series of electron diffraction patterns and dark-field images obtained from alloys kept at 1173 K for 100 h. All of the images were taken under the electron incidence parallel to the [001] axis. The images of the alloys with $x = 0.40$ and 0.60 were taken by using the $D0_{22}$ ordered spots ($\frac{1}{2}10$ spots). In both of these images, the bright-contrast regions correspond to one of the $D0_{22}$ variants. The dark-field images of the alloys with $x = 0.42$, 0.45, 0.50, and 0.52 were taken by using the $L1_2$ ordered spots (100 spots). As for the alloy with $x = 0.55$, the dark-field image was taken by using the $L1_2$ ordered spots (100 spots), and the inset is a dark-field image taken by using the $D0_{22}$ ordered spots ($\frac{1}{2}10$ spots).

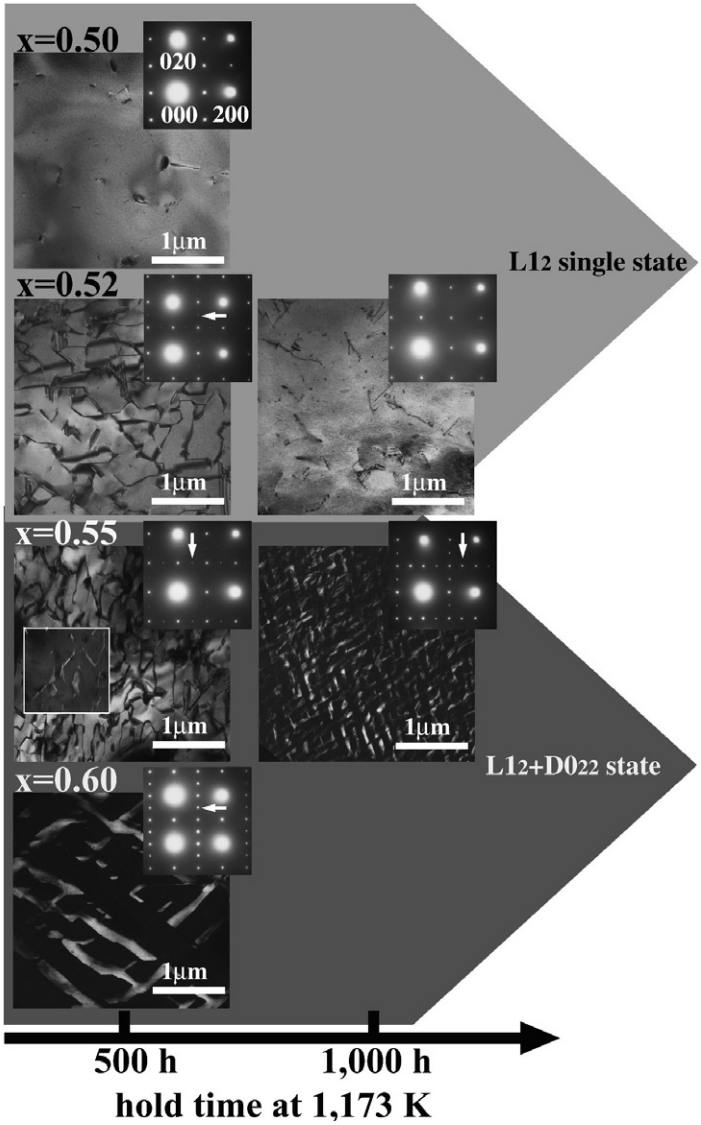

Figure 3. Temporal development of the microstructures of quenched $Ni_3Al_{1-x}V_x$ alloys with $x = 0.50$, 0.52, 0.55 and 0.60 while being kept at 1173 K for up to 1000 h. The observation was carried out under the electron incidence parallel to the [001] axis. The images obtained from the alloys with $x = 0.50$ and 0.52 were taken by using 100 ordered spots. As for the alloy with $x = 0.55$, the main image and the inset of the state after a hold time of 500 h were taken by using 100 and $\frac{1}{2}$10 spots, respectively, while that of the state after a hold time of 1000 h was taken by using a $\frac{1}{2}$10 spot. The dark-field image obtained from the alloy with $x = 0.60$ was also taken by using a $\frac{1}{2}$10 spot.

are not observed. These results indicate that the final state of the alloy with $x = 0.50$ is the $L1_2$ single state. As for the alloy with $x = 0.52$, the state obtained at a hold time of 500 h basically includes many APBs. As shown in the corresponding diffraction pattern, the $D0_{22}$ ordered spots appear with very weak intensities. This indicates that the alloy is still in the $L1_2 + D0_{22}$ state even after holding it at 1173 K for 500 h. Upon increasing the hold time to 1000 h, however,

the $D0_{22}$ regions were annihilated and the $L1_2$ single state with few APBs was obtained. Such a change in the microstructures is similar to that observed for the alloy with $x = 0.50$. We therefore conclude that the final state of the alloy with $x = 0.52$ is also the $L1_2$ single state.

The process for the formation of the $L1_2$ single state (i.e., the transient appearance of the $D0_{22}$ regions, subsequent formation of APBs, and the deterioration of the APB density) coincides well with that of the alloy with $x = 0.48$. The only difference is that the formation time of the autoregressive $L1_2$ single state becomes longer as the V content of the alloy increases. In the alloy with $x = 0.55$, on the other hand, an increase in the intensities of the $D0_{22}$ ordered spots with the passage of time is indicative of the evolution to the $L1_2 + D0_{22}$ state. Actually, we can observe that the $D0_{22}$ regions appear in the vicinity of the APBs (see the alloy with a 500 h hold time) and grow further with a longer hold time, resulting in the formation of the $L1_2 + D0_{22}$ checked pattern with the $\{110\}$ habit planes (see the alloy with a 1000 h hold time). It is thus clear that the alloy with $x = 0.55$ heads for the $L1_2 + D0_{22}$ equilibrium state in the isothermal process. Note that a similar checked pattern obtained after a hold time of 100 h in the alloy with $x = 0.60$ evolves in terms of the grain growth of the $D0_{22}$ regions as the hold time is lengthened (see the state of the 500 h hold-time alloy with $x = 0.60$). From these results, it is found that the final state of the phase separation varies with the change in the V content, i.e., $x = 0.40$ results in the $L1_2 + D0_{22}$ state, $0.40 < x < 0.55$ in the metastable $L1_2$ single state, and $x \geqslant 0.55$ in the $L1_2 + D0_{22}$ state. This variation is experimental evidence that a bifurcation of the final states takes place in the evolution of states of the $Ni_3Al_{1-x}V_x$ alloy system under the present thermodynamic treatment.

3.2. Difference in the kinetic processes leading to the variation in the final states

The above-mentioned results revealed that the formation of the final states was closely related to the differences in the initial $L1_2$ microstructures. Concretely, cuboidal domains with an average size of more than 100 nm on a side ($0.40 < x < 0.55$) stagnated $D0_{22}$ precipitation, whereas precipitation resulting in the formation of the $L1_2 + D0_{22}$ state progressed with smaller ($x \geqslant 0.55$) or no domains ($x = 0.40$). In order to make clear the kinetic processes that cause the bifurcation of the final states, we focus our attention here on the differences in the nucleation sites and in the formation processes of the $L1_2/D0_{22}$ habit plane with respect to the variation in the initial microstructures. It should be mentioned here that the misfit of the lattice parameters between the $D0_{22}$ and $L1_2$ structures requires the formation of the habit plane on the $\{110\}$ planes in the equilibrium $L1_2 + D0_{22}$ state [10, 11].

Figure 4 compares the microstructures of the alloys with $x = 0.40$ (no cuboidal domains), 0.50 (large cuboidal domains) and 0.60 (small cuboidal domains) at the initial stage of the microstructure evolution. Figure 4(a) shows a set of bright- and dark-field images obtained from the alloy with $x = 0.40$. In the dark-field image, we can see that the $D0_{22}$ regions appear in the vicinity of the partial dislocations. This indicates that these dislocations serve as the nucleation sites of the $D0_{22}$ regions in this alloy. An important feature of the microstructure is that the $D0_{22}$ regions extend along and/or perpendicular to the dislocations, i.e., one of the $\langle 110 \rangle$ directions. There are no restrictions therefore on the formation of the $\{110\}$ habit planes when the regions grow in that direction, resulting in the attainment of the $L1_2 + D0_{22}$ equilibrium state. In the case of the alloys with $x = 0.50$ and 0.60, on the other hand, the $D0_{22}$ regions nucleate at the small-angle tilt boundaries.

Figures 4(b) and (c) show dark-field images obtained from these two alloys, respectively. In these images, it is clearly seen that the $D0_{22}$ regions appear at the small-angle tilt boundaries. This stems from the fact that segments of the small-angle tilt boundaries have the $D0_{22}$ atomic configuration. It should be noted here that the domain size directly dominates the

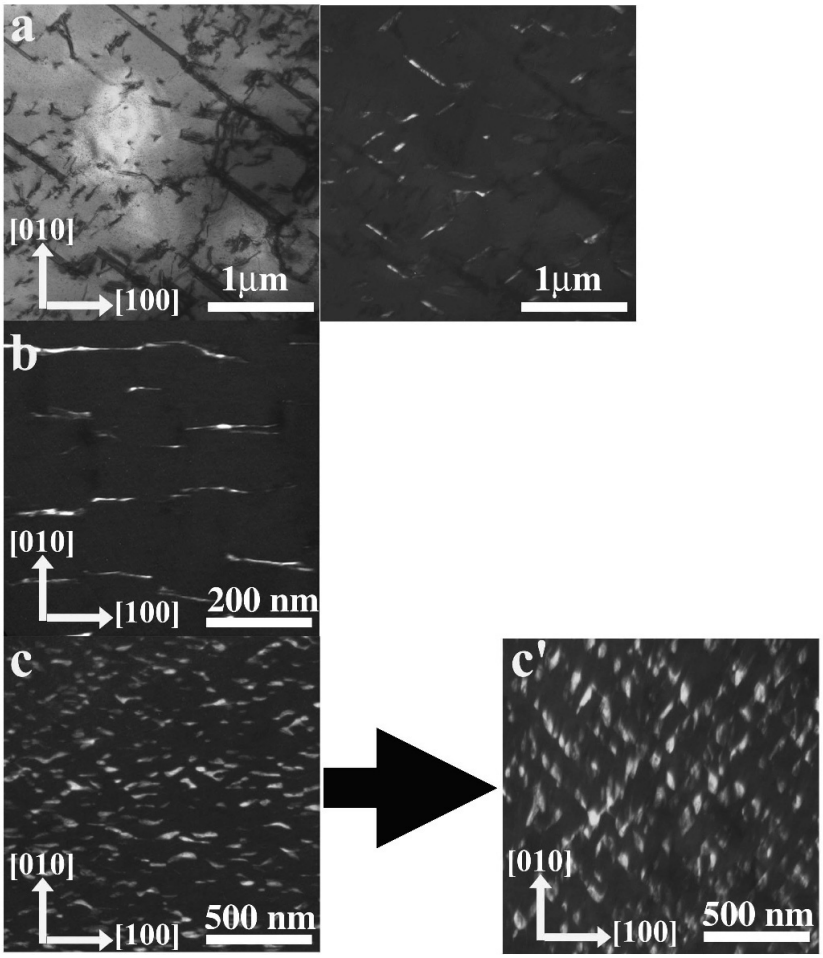

Figure 4. A comparison of the microstructure evolution at the initial stages of the $Ni_3Al_{1-x}V_x$ alloys. All of the images were taken under the electron incidence parallel to the [001] axis and the dark-field images were taken by using the $\frac{1}{2}10$ ordered spots in the respective diffraction patterns. (a) A set of bright- and dark-field images obtained from the alloy with $x = 0.40$ and kept at 1173 K for 10 min. (b) A dark-field image obtained from the alloy with $x = 0.50$ and kept at 1173 K for 10 min. (c) and (c′) Dark-field images obtained from the alloy with $x = 0.60$ and kept at 1173 K for 10 min and 30 min, respectively.

morphological features of the $D0_{22}$ regions. Concretely, the length of the $D0_{22}$ regions depends on the domain size, and their density increases with an increasing number of small-angle tilt boundaries. A notable difference in the kinetic process of these alloys from that of the alloy with $x = 0.40$ is that the change in the habit planes from the $\{100\}$ to $\{110\}$ planes must take place to form the $L1_2 + D0_{22}$ state. In the alloy with $x = 0.50$, the atomic migration cannot follow the change in the habit planes. The reason is that diffusion blocking suppresses the long-range atomic migration (about 200 nm) in the $L1_2$ matrix, resulting in the annihilation of the $D0_{22}$ regions (the detailed kinetic process, including the atomistic model, is described in [4]). In the case of the alloy with $x = 0.60$, however, the initial $D0_{22}$ regions are short because the cuboidal domains of the initial microstructure are sufficiently small. The advantage of such shortness is that the change in the habit planes can proceed under relatively short-range atomic migration

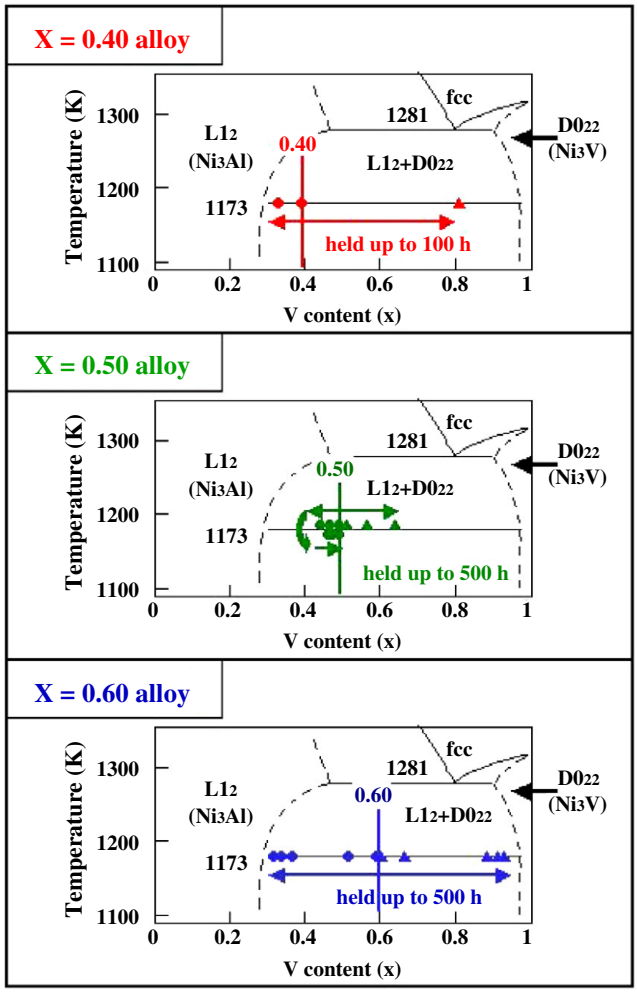

Figure 5. V-content variations obtained from the alloys with $x = 0.40$, 0.50, and 0.60, respectively. In order to compare the measured values with the equilibrium ones, the data are embedded in the phase diagram of the $Ni_3Al_{1-x}V_x$ alloy system. Note that each value is an average of 15 measured values.

(about 20 nm). For instance, the initial $D0_{22}$ regions in this alloy can rearrange from the ⟨100⟩ to ⟨110⟩ directions before they grow so large (see figure 4(c′)). Thus, a marked blocking effect does not appear and the $L1_2 + D0_{22}$ equilibrium state with the {110} habit planes can form at a later stage by utilizing the small boundaries available. These microstructure changes indicate that the variation in the initial microstructures substantially impacts the changes in the nucleation sites of the $D0_{22}$ regions and in subsequent processes to form the {110} habit planes between the $L1_2$ and $D0_{22}$ structures. It is understood that three types of kinetic processes lead the systems to their respective final states, resulting in the bifurcation of the final states.

We will simply mention here the change in the chemical compositions related to the three types of processes. Figure 5 shows the changes in the average V content of both the $D0_{22}$ regions and the $L1_2$ matrix of the alloys with $x = 0.40$, 0.50, and 0.60 during the isothermal hold. The temporal change in the average values is embedded in the phase diagram of the $Ni_3Al_{1-x}V_x$

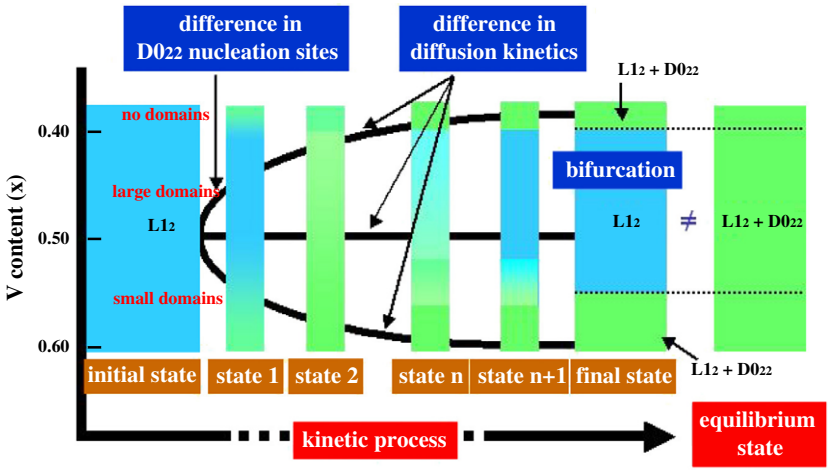

Figure 6. Bifurcation diagram of the temporal evolution of states in the phase separation of the $Ni_3Al_{1-x}V_x$ alloy system ($0.40 \leqslant x \leqslant 0.60$). The blue colour represents the $L1_2$ state while the green colour corresponds to the $L1_2 + D0_{22}$ state.

alloy system. In the case of the alloys with $x = 0.40$ and 0.60, the data clearly indicate that the phase separation is accompanied by a distribution of the V content. Specifically, the long-range atomic diffusion basically dominates the kinetic process of the phase separation in both alloys, although their microstructure change is quite different. On the other hand, the stagnation of the phase separation is characterized by the reversible-like variation of the V content in the $L1_2$ matrix, as shown in the case of the alloy with $x = 0.50$. This characteristic coincides well with the V content variation observed in the alloy with $x = 0.48$ [4]. It is thus understood that diffusion blocking in the $L1_2$ matrix is dominant in the formation of the $L1_2$ single state.

4. Discussion

In this study, it was experimentally found that differences in the initial microstructures and respective kinetic processes in the evolution of states caused a bifurcation of the final states in the phase separation of the $Ni_3Al_{1-x}V_x$ alloy system. On the basis of the experimental results, we will first draw an overall picture of this peculiar phase separation. Figure 6 shows a bifurcation diagram in the evolution of states related to $D0_{22}$ precipitation in the supersaturated $L1_2$ matrix. Because the atomic environment of the microstructure in the initial state controls the atomic migration in the next instant, the formation of the microstructure at state 1 is based on the initial microstructure. In the same way, the microstructure at state 1 (or state n) dominates the evolution to state 2 (or state $n + 1$). Thus, the kinetic process in the evolution of states is basically dominated by every momentary state, beginning with the initial one. In the present study, it was found that the initial microstructure varied among the alloys with $0.40 \leqslant x \leqslant 0.60$ and that the nucleation sites of the $D0_{22}$ regions varied depending on the initial microstructures. The difference in the nucleation sites then gave rise to three formation patterns of the $L1_2/D0_{22}$ habit plane and each pattern led the states to their corresponding final one. This diagram clearly indicates that the difference in the initial microstructures was augmented during the respective kinetic processes, resulting in the bifurcation of the final states.

Here we simply mention the reason why the $L1_2$ single state (not the $D0_{22}$ single state) is formed as a final metastable state. It is considered that the formation of the $L1_2$ single state depends closely on the stability between the $L1_2$ and the $D0_{22}$ structures. As is well known, the

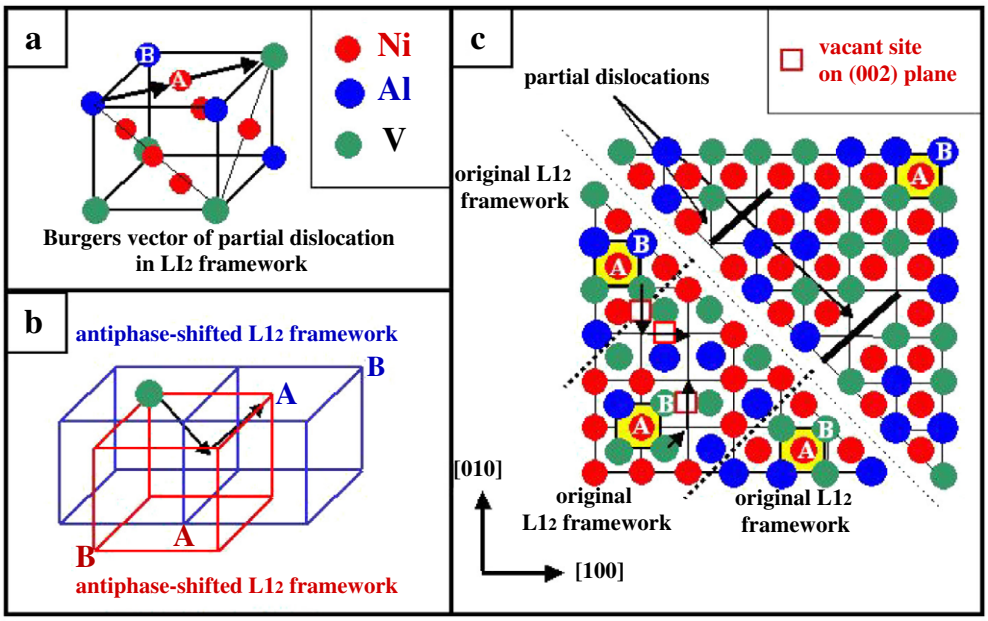

Figure 7. (a) Schematic diagram depicting the Burgers vector of a partial dislocation in the $L1_2$ structure. The A and B sites correspond to the face-centred and edge sites in the $L1_2$ frameworks. (b) Schematic diagram of the original $L1_2$ framework (red) and the $\langle\bar{1}10\rangle$ antiphase-shifted one (blue). The V atom migration along the B $\rightarrow$ A $\rightarrow$ B sites in the original $L1_2$ framework is depicted by the arrows. It should be noticed that this migration corresponds to the A $\rightarrow$ A $\rightarrow$ A jumps in the antiphase-shifted framework. (c) A conceivable model of the V atom migration in the vicinity of the partial dislocations. The yellow cells represent the $L1_2$ units of the respective regions. For simplicity, antisite defects are ignored and vacancies are located only at the A sites in the diagram.

$D0_{22}$ structure can be regarded as a long-period superstructure characterized by the periodic array of the antiphase boundaries introduced in the $L1_2$ structure. In this regard, the energies of the $L1_2$ and $D0_{22}$ structures were estimated with respect to the number of valence electrons per atom (e/a) [13, 14]. It was found that the $D0_{22}$ structure was stable when e/a was larger than 8.60, while e/a smaller than 8.60 stabilized the $L1_2$ structure. The e/a values of the alloys with $x = 0.40$ and 0.60 were estimated to be 8.45 and 8.55, respectively. On this basis, it is assumed that the $L1_2$ single state rather than the $D0_{22}$ one was preferred in the event that the alloys with $0.40 < x < 0.55$ had to drop into a certain metastable state. The fact that the quenched state (initial metastable state) of the alloys with $x \leqslant 0.60$ was basically the $L1_2$ single one provides strong support for the application of the e/a classification to $Ni_3Al_{1-x}V_x$ alloys.

Let us discuss the details of the diffusion kinetics of the respective processes from an atomistic viewpoint. As has been reported previously, the formation of the metastable $L1_2$ single state (in the case of the alloys with $0.40 < x < 0.55$) depends on the occurrence of diffusion blocking in the $L1_2$ structure during the kinetic process (refer to figure 8 in [4] for the atomistic model describing diffusion blocking). Because its occurrence correlates well with the small probability of V atoms jumping from A to B sites in the $L1_2$ structure, a decrease in the vacant sites during the isothermal process should be taken into account. When the alloys were quenched in ice water from 1623 K, it is thought that the equilibrium vacancy composition at that temperature should have been almost entirely preserved in the quenched alloys.

On the other hand, the equilibrium vacancy concentration at a holding temperature of 1173 K was smaller than that at 1623 K. On the basis of theoretical calculations [8, 12], it is

estimated that the equilibrium vacancy concentration of the alloy with $x = 0.50$ and kept at 1173 K was of the order of 10^{-7} at the A sites and 10^{-9} at the B sites, while that of the alloy kept at 1623 K (disordered fcc structure) was of the order of 10^{-5}. This means that the vacancy composition at the B sites in the $L1_2$ matrix decreased by approximately an order of four during the isothermal process. Since the B-site atoms mainly migrated within the $L1_2$ domains, the decrease in the vacant B sites undoubtedly had a large effect on the diffusion kinetics. This is because the annihilation of the vacant B sites directly reduces the probability of the A $\rightarrow$ B jump of the V atoms. Actually, in the alloys with $0.40 < x < 0.55$, the long-range atomic diffusion leading to the formation of the $D0_{22}$ regions occurred in the supersaturated $L1_2$ matrix only at the initial stage (see figure 5). In other words, the decrease in the vacant B sites gave rise to diffusion blocking. It can thus be inferred that the migration paths of the V atoms within the large $L1_2$ domains are severely affected when the vacant B sites are annihilated. Note that large $L1_2$ grains with few lattice defects were typical of the final state when the phase separation was stagnated by the blocking effect.

When the $L1_2$ domains are small enough (in the case of the alloys with $0.55 \leqslant x \leqslant 0.60$) or when many pairs of partial dislocations are present in the $L1_2$ grains (in the case of the alloy with $x = 0.40$), the decrease in the vacant B sites does not have such a large impact on the atomic migration. In the former case, the short-range atomic migration is sufficient for the nucleation of the $D0_{22}$ regions and the formation of the $L1_2/D0_{22}$ habit plane when the many small-angle tilt boundaries are used effectively (see figures 4(c) and (c′)). It should also be pointed out here that a larger V content increases the probability of V atoms encountering the few vacant B sites available. In the latter case, the region between two partial dislocations as well as the space created by the dislocations can be utilized as atomic migration paths.

Figure 7 shows a schematic diagram of the atomic configuration and one conceivable model of V atom migration in the vicinity of a pair of partial dislocations. For simplicity, only the migration process of the V atoms is depicted in the diagrams. As has been mentioned, the partial dislocations were present mainly along one of the $\langle 110 \rangle$ directions in the $L1_2$ matrix. Because the Burgers vector of one partial dislocation is one of the $\frac{1}{2}\langle \bar{1}10 \rangle$ directions, as shown in figure 7(a), the atomic configuration of the region between two partial dislocations is normally characterized by antiphase atomic displacement in that direction from the original $L1_2$ one. An important feature of V atom migration is that the B $\rightarrow$ A $\rightarrow$ B jumps in the original $L1_2$ framework coincide with the A $\rightarrow$ A $\rightarrow$ A jumps in the antiphase-shifted $L1_2$ framework (see figure 7(b)). Note that the vacant A sites are much larger in number than the vacant B sites in the $L1_2$ structure. Therefore, even after the vacant B sites are annihilated during the isothermal process, atomic diffusion based on the A $\rightarrow$ A $\rightarrow$ A jumps in the antiphase-shifted regions can promote the long-range migration of V atoms without disturbing the original $L1_2$ configuration (see figure 7(c)). This atomistic model clearly implies that topological defects can locally break the selectivity of the vacant sites in the large $L1_2$ grains and that the long-range V atom migration can occur by using the vacant sites in the antiphase-shifted regions. This discussion strongly suggests that the sensitivity of the main V atom migration paths to the annihilation of the vacant B sites in the $L1_2$ matrix is a crucial factor in the diffusion kinetics.

The evolution of states characterized by the bifurcation diagram is obviously beyond the theoretical framework that has traditionally described the phase separation of alloys. Our results reveal that the bifurcation of the final states originates in the difference in the initial microstructures and the respective kinetic processes. In general, the kinetics of the phase separation is described on the assumption that alloys are in a closed system, with no incoming or outgoing of matter such as atoms from or to their surroundings. However, the annihilation of vacant sites basically occurs in alloys accompanied by a decrease in the vacancy compositions from the supersaturated to equilibrium ones. In the present case, the annihilation of the vacant B

sites during the isothermal process plays a crucial role in the diffusion kinetics and consequent evolution of states.

When the annihilation of the vacant B sites substantially affects the migration paths, the system heads for the metastable $L1_2$ single state. On the other hand, if the annihilation has a negligible effect, the system heads to the equilibrium $L1_2 + D0_{22}$ state, as can be expected from the phase diagram. The overall picture derived from our experimental results strongly suggests that the diffusion kinetics dominating the evolution of states should be treated as an 'open system' in terms of the annihilation of the vacant B sites under the present thermodynamic condition. In conclusion, the bifurcation of the final states is experimental evidence that indicates the application of a closed-system approximation to the phase separation of alloys is limited when the diffusion field exhibits a severe selectivity of crucial vacant sites.

5. Conclusion

The kinetics of the phase separation in alloys is generally dominated by the long-range atomic diffusion. Therefore, the kinetic process arouses our interest when the diffusion field essentially possesses a certain restraint on atomic migration. Because vacancies play a crucial role in atomic migration, a severe selectivity of vacant sites can produce such a restraint. From this perspective, we have experimentally investigated the evolution of states related to $D0_{22}$ precipitation in the supersaturated $L1_2$ matrix to form the $L1_2 + D0_{22}$ equilibrium state of the $Ni_3Al_{1-x}V_x$ $(0.40 \leqslant x \leqslant 0.60)$ alloy system. As a result, it has been found that the initial $L1_2$ microstructure varied accompanying the change in the V content and that such a variation caused a bifurcation of the final states, i.e., the $L1_2 + D0_{22}$ equilibrium state ($x = 0.40$ and $x \geqslant 0.55$) and the metastable $L1_2$ single state ($0.40 < x < 0.55$). A detailed analysis revealed that three types of kinetic processes originated from the variation in the initial microstructures and led the states to their corresponding final one. A characteristic of the kinetic processes is the sensitivity of atomic migration to a decrease in the crucial vacant sites in the $L1_2$ matrix during the isothermal treatment. The sensitivity is dependent on the initial microstructure and determines whether diffusion blocking occurs in the $L1_2$ matrix. This strongly suggests that such sensitivity is a crucial factor for describing the diffusion kinetics and the subsequent evolution of states. On this basis, it is concluded that the diffusion kinetics originating the bifurcation of the final states in the present phase separation should be treated as an open system in terms of the annihilation of vacancies.

Acknowledgment

One of the authors (MT) acknowledges the technical support of T Doi at Waseda University.

References

[1] Sato H and Kikuchi R 1983 *Phys. Rev.* B **28** 648
[2] Sato H, Ishikawa T and Kikuchi R 1985 *J. Phys. Chem.* **46** 1361
[3] Tanimura M, Kikuchi M and Koyama Y 2002 *J. Phys.: Condens. Matter* **14** 7053
[4] Tanimura M, Hirata A and Koyama Y 2004 *Phys. Rev.* B **70** 094111
[5] Xu J-H, Oguchi T and Freeman A J 1987 *Phys. Rev.* B **36** 4186
[6] Kim S M 1991 *J. Mater. Res.* **6** 1455
[7] Numakura H, Ikeda T, Koiwa M and Almazouzi A 1998 *Phil. Mag.* A **77** 887
[8] de Koning M 2002 *Phys. Rev.* B **66** 104110
[9] Hong Y, Mishima Y and Suzuki T 1989 *Mater. Res. Soc. Symp. Proc.* **133** 429
[10] Poduri R and Chen L-Q 1998 *Acta Mater.* **46** 1719
[11] Bendersky L A, Biancaniello F S and Williams M E 1994 *J. Mater. Res.* **9** 3068
[12] Badura-Gergen K and Schaefer H-E 1997 *Phys. Rev.* B **56** 3032
[13] Lin W, Xu J-H and Freeman A J 1992 *Phys. Rev.* B **45** 10863
[14] Cabet E, Pasturel A, Ducastelle F and Loiseau A 1996 *Phys. Rev. Lett.* **76** 3140